JOURNAL OF VIROLOGY, Sept. 1998, p. 7228–7236 Vol. 72, No. 9
0022-538X/98/$04.00+0

Rotavirus Infection Reduces Sucrase-Isomaltase Expression in Human Intestinal Epithelial Cells by Perturbing Protein Targeting and Organization of Microvillar Cytoskeleton

NATHALIE JOURDAN,[1] JEAN PHILIPPE BRUNET,[1] CATHERINE SAPIN,[2] ANNE BLAIS,[1] JACQUELINE COTTE-LAFFITTE,[1] FRANÇOISE FORESTIER,[1] ANNE-MARIE QUERO,[1] GERMAIN TRUGNAN,[2] AND ALAIN L. SERVIN[1]*

Institut National de la Santé et de la Recherche Médicale, CJF 94 07, Pathogénie Cellulaire et Moléculaire des Microorganismes Entérovirulents, Faculté de Pharmacie, Université Paris XI, 92296 Chatenay-Malabry Cedex,[1] and CJF 96 07, Signalisation Moléculaire et Physiopathologie de l'Adressage des Protéines dans les Cellules Épithéliales, Faculté de Médecine Saint Antoine, Université Paris VI, 75012 Paris,[2] France

Received 17 March 1998/Accepted 29 May 1998

Rotavirus infection is the most common cause of severe infantile gastroenteritis worldwide. These viruses infect mature enterocytes of the small intestine and cause structural and functional damage, including a reduction in disaccharidase activity. It was previously hypothesized that reduced disaccharidase activity resulted from the destruction of rotavirus-infected enterocytes at the villus tips. However, this pathophysiological model cannot explain situations in which low disaccharidase activity is observed when rotavirus-infected intestine exhibits few, if any, histopathologic changes. In a previous study, we demonstrated that the simian rotavirus strain RRV replicated in and was released from human enterocyte-like Caco-2 cells without cell destruction (N. Jourdan, M. Maurice, D. Delautier, A. M. Quero, A. L. Servin, and G. Trugnan, J. Virol. 71:8268–8278, 1997). In the present study, to reinvestigate disaccharidase expression during rotavirus infection, we studied sucrase-isomaltase (SI) in RRV-infected Caco-2 cells. We showed that SI activity and apical expression were specifically and selectively decreased by RRV infection without apparent cell destruction. Using pulse-chase experiments and cell surface biotinylation, we demonstrated that RRV infection did not affect SI biosynthesis, maturation, or stability but induced the blockade of SI transport to the brush border. Using confocal laser scanning microscopy, we showed that RRV infection induces important alterations of the cytoskeleton that correlate with decreased SI apical surface expression. These results lead us to propose an alternate model to explain the pathophysiology associated with rotavirus infection.

Rotaviruses, members of the *Reoviridae* family, exhibit a marked tropism for the differentiated enterocytes of the intestinal epithelium (5) and are recognized as the leading cause of infantile viral gastroenteritis worldwide (35). Although much is known about their replication and maturation processes, the pathophysiologic mechanisms by which rotavirus infection induces diarrhea remain unclear. Extensive studies using animal models have reported the presence of mild to severe histopathologic changes and functional abnormalities in infected intestinal mucosa, depending on the virulence of the strain (for a review, see reference 26). Whatever the severity of histopathologic changes, the activities of disaccharidases (sucrase-isomaltase [SI], lactase, and maltase-glucoamylase) are frequently decreased by rotavirus infection (11, 18). It was previously thought that this phenomenon was due to the destruction of mature enterocytes of the villus tips (18). However, this hypothesis cannot explain low disaccharidase activities in the absence of enterocyte destruction (4, 17).

To gain further insight into the mechanism by which rotavirus infection induces a decrease in disaccharidase activities, an in vitro system representing mature enterocyte would be beneficial. The human intestinal epithelial cell line Caco-2 was established from a human colon adenocarcinoma (20). Confluent cultures of these cells exhibit many of the morphologic and biochemical properties of mature enterocytes (55). These cells are polarized, exhibiting a brush border membrane on their apical surface that expresses a variety of enterocytic hydrolases. In previous work, we used these cells to demonstrate that the simian rotavirus strain RRV was able to replicate and be released from Caco-2 cells without cell destruction, in accordance with some in vivo observations (34).

Among the four brush border disaccharidases expressed in the small intestine, SI, a heterodimer complex which hydrolyzes maltose, maltotriose, and sucrose, has been extensively studied in vivo as well as in the enterocyte-like model Caco-2 (for a review, see reference 28). SI complex is synthesized as a single precursor starting from the N terminus of isomaltase (33). In the endoplasmic reticulum, SI is cotranslationally N-glycosylated to give an immature and inactive high-mannose precursor (43). During passage through the Golgi apparatus, SI is processed to a fully active mature complex glycosylated form (43). Then, SI is directly targeted from the trans Golgi network (TGN) to the apical membrane (42). This feature distinguishes SI from several other brush border hydrolases that are first delivered basolaterally and then delivered to the apical pole by transcytosis, as is the case for dipeptidyl peptidase IV (DPP IV) (36, 42). SI activity can be regulated by several different mechanisms. Decrease of SI activity at the mRNA level has been induced by change in glucose metabolism (8, 57), high-carbohydrate diet (7, 23, 24), and thyroxin or glucocorticoid treatment (38, 64). SI activity can also be reduced by posttranslational events (61). Defect of processing (folding and glycosylation), intracellular transport, or insertion

* Corresponding author. Mailing address: CJF INSERM 94 07, Faculté de Pharmacie, 5 rue J. B. Clément, 92296 Chatenay-Malabry Cedex, France. Phone and fax: 33-1 46 83 56 61. E-mail: alain.servin@cep.u-psud.fr.

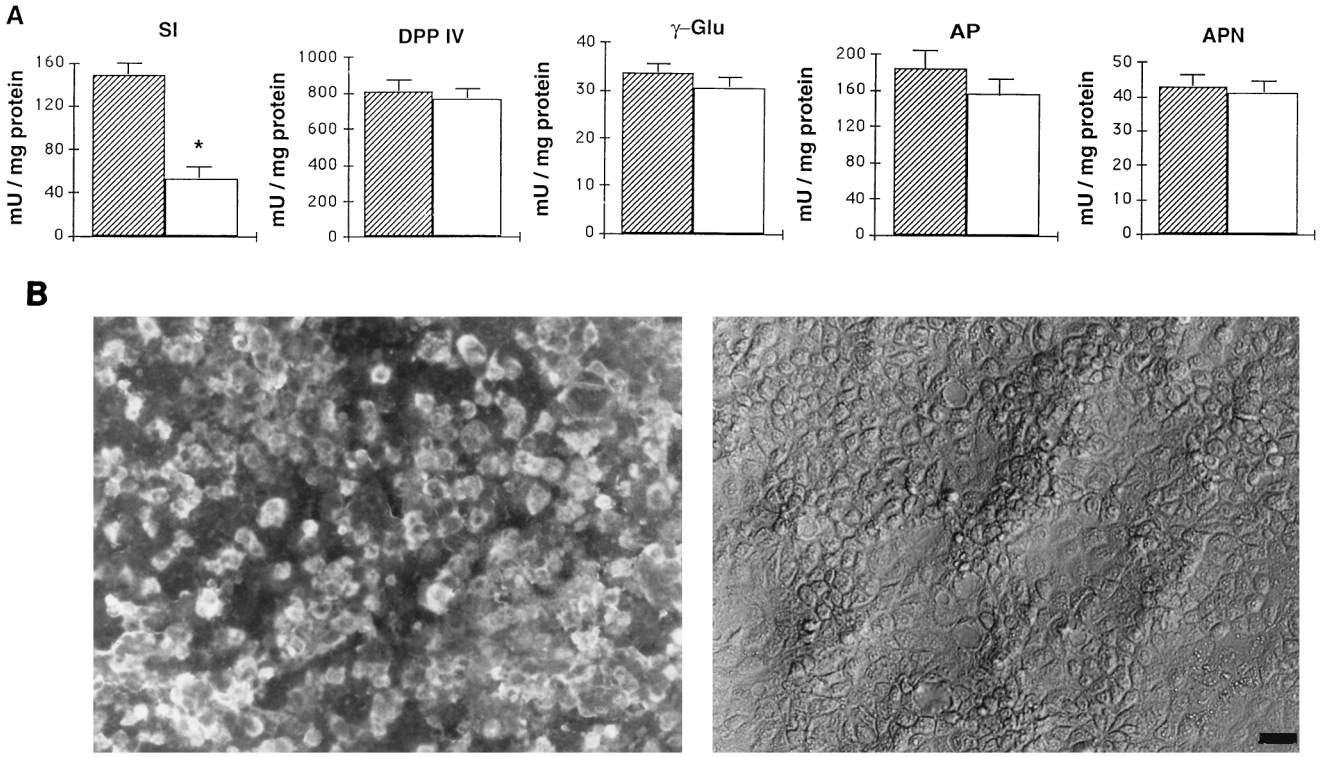

FIG. 1. Enzyme activity and RRV antigen expression in Caco-2 cells infected with RRV. (A) At 24 h p.i., total membrane fraction was prepared and assayed for SI, DPP IV, γ-GTP (γ-Glu), APN, and AP activities. Each bar represents the mean ± SD of six experiments. *, statistically significant difference ($P < 0.01$). Additional determination of enzymatic activity indicates that SI activity decreased from 16 to 24 h (not shown). ▨, control; □, RRV infected. (B) At the same times p.i., infected cells were fixed with 3% paraformaldehyde and permeabilized with Triton X-100. RRV antigens were immunostained with a polyclonal anti-group A rotavirus and fluorescein-labeled anti-rabbit IgG secondary antibodies (left). Infected monolayers were also examined by phase-contrast microscopy (right). The bar indicates 25 μm.

of the enzyme into the brush border membrane are associated with congenital SI deficiency (21, 29, 40, 54). Abnormality in SI glycosylation leading to degradation by rapid proteolytic breakdown has also been induced experimentally by fructose and sucrose (15, 16), epidermal growth factor EGF (13), or heat shock (56) treatment of Caco-2 cells. Impairment of SI anchorage in the brush border of Caco-2 cells has also been induced by brush border cytoskeletal alteration (12).

In this work, we studied the regulation of SI expression in RRV-infected Caco-2 cells. We found that SI activity and apical expression were specifically and selectively decreased by RRV infection in the absence of cell destruction. Using pulse-chase experiments and cell surface biotinylation, we demonstrated that RRV infection did not affect SI biosynthesis, maturation, or stability but induced the block of SI transport from the TGN to brush border membrane. Using confocal laser scanning microscopy (CLSM), we found that RRV infection induces an important alteration of the brush border-associated cytoskeleton that correlates with decreased SI apical surface expression. These results lead us to propose an alternate rotavirus pathophysiological model in which alteration of enterocytic functions depends on perturbation in protein trafficking and cytoskeleton.

MATERIALS AND METHODS

Reagents. Leupeptin, aprotinin, antipain, benzamidine, pepstatin A, phenylmethylsulfonyl fluoride, Gly-Pro *p*-nitroanilide, L-Ala *p*-nitroanilide, *p*-nitrophenylphosphate, 4-aminoantipyrine, glucose oxidase, peroxidase, trypsin, Triton X-100, salicylic acid, 1,4-diazabicyclo-(2.2.2.)octane (DABCO), and paraformaldehyde were purchased from Sigma-Aldrich Chimie SARL, L'Isle d'Abeau Chesnes, France. Glycergel and propidium iodide were from Dakopatts, Copenhagen, Denmark. Ammonium chloride, methanol, and acetic acid were obtained from Prolabo, Paris, France. Protein A-Sepharose beads were purchased from Pharmacia Biotech, Saclay, France. Products for cell culture were from Life Technologies, Eragny, France, except Dulbecco modified Eagle's medium (DMEM) without methionine and cysteine, which was obtained from ICN Biomedicals Inc., Costa Mesa, Calif. Costar Transwell filters (0.4-μm pore size) were obtained from Dominique Dutscher, Brumath, France. The bicinchoninic acid assay kit, NHS-LC-biotin, and streptavidin-agarose beads (all manufactured by Pierce) were purchased from Interchim, Montluçon, France. Pansorbin beads were from Calbiochem via France Biochem, Meudon, France. 70% L-[^{35}S]methionine–30% cysteine (PRO-MIX) was obtained from Amersham, Les Ulis, France. Endoglycosidase H (endo H) was provided by Genzyme (Tebu, Le Perray en Yveline, France).

Cells and culture conditions. The Caco-2 cell line was established from a human colon adenocarcinoma by J. Fogh (20). Cells were cultured (passages 60 to 90) in DMEM supplemented with 20% heat-inactivated fetal bovine serum (FBS), antibiotics (100 U of penicillin and 100 μg of streptomycin per ml), and 1× nonessential amino acids (55). For viral infection studies, the cells were seeded at a density of 10,000 c/cm^2 on tissue culture-treated polycarbonate Transwell filters containing pores of 0.4-μm diameter. Apical and basal media were replaced every 2 days. Infections were done late after confluency, i.e., after 20 days in culture. The cells were maintained at 37°C in a 10% CO_2–90% air atmosphere. MA104 cells were cultured in minimal essential medium supplemented with 10% FBS, 2 mM glutamine, antibiotics (20 U of penicillin and 40 U of streptomycin per ml), and 1× nonessential amino acids in a 5% CO_2 incubator. Cells (10^5/cm^2) were seeded in 150-cm^2 tissue culture flasks (Falcon; Becton Dickinson, LePont-de-Claix, France) and used for production of virus stock 48 h later.

Virus. Rhesus rotavirus RRV was obtained from Jean Cohen (Institut National de la Recherche Agronomique, Jouy en Josas, France). Virus stock was generated in MA104 cells after 24-h preincubation of the cells in a serum-free culture medium. Viruses were activated by treatment with 0.5 μg of trypsin per ml (9) at 37°C for 30 min, and MA104 cell monolayers were infected at a multiplicity of infection of 0.002 PFU/cell. After 1 h of adsorption at room temperature, the inoculum was removed and infected cells were incubated in culture medium containing 0.5 μg of trypsin per ml. After a complete cytopathic effect was obtained, the cultures were freeze-thawed and cell debris was removed by centrifugation.

Virus infection of Caco-2 cells. Caco-2 cells grown on Transwell filters (cultured without FBS during 24 h) were infected with an inoculum of activated

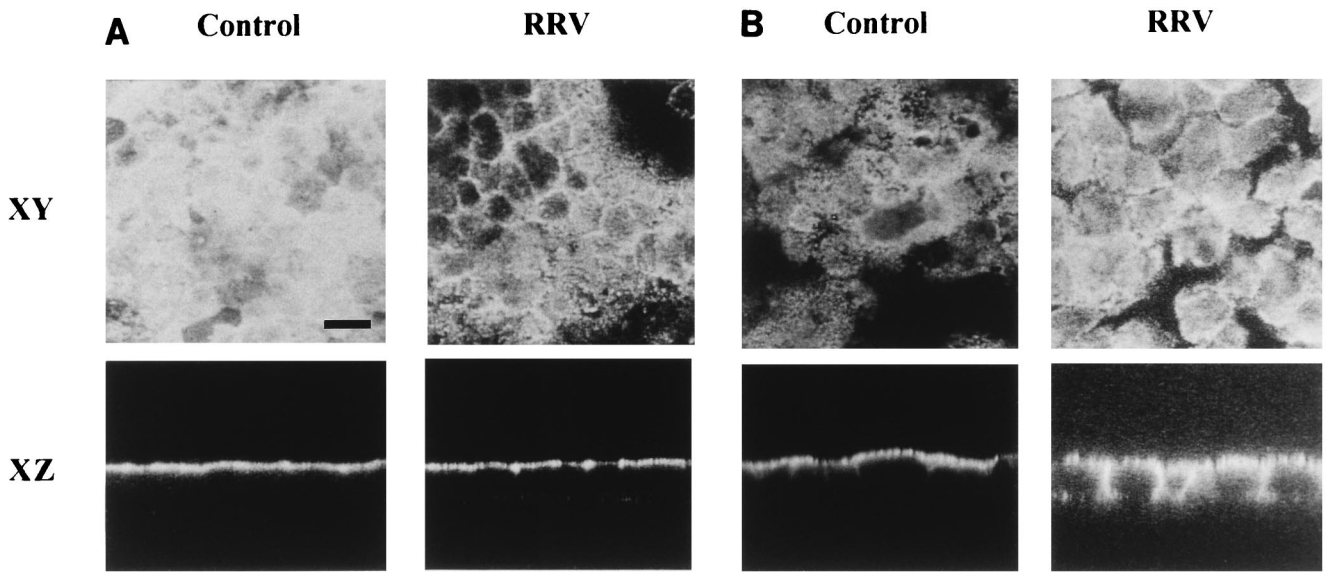

FIG. 2. Alteration in the apical SI distribution in RRV-infected Caco-2 cells. At 24 h p.i., RRV-infected and mock-infected Caco-2 cells were fixed and permeabilized as described for Fig. 1. (A) SI was stained with a rat anti-SI MAb and fluorescein-coupled anti-rat IgG secondary antibodies. (B) DPP IV was immunostained with a rat anti-DPP IV MAb and fluorescein-coupled anti-rat IgG secondary antibodies. Horizontal (XY) sections at the apical level and vertical (XZ) sections were obtained by direct confocal analysis. Each bar indicates 10 μm.

RRV at a multiplicity of infection of 10 PFU/cell in apical chambers for 1 h at room temperature. The inoculum was then removed, and fresh medium containing 0.5 μg of trypsin per ml was added. Infected cells were incubated at 37°C in a 10% CO_2–90% air atmosphere and were processed for experiments at the indicated time postinfection (p.i.).

Enzyme assays. Cells were washed in ice-cold phosphate-buffered saline (PBS), scraped off, suspended in PBS, and homogenized. Enzyme activities were measured in enriched total membrane fraction following centrifugation of the cell homogenates (1 h, 100,000 × *g*, 4°C) (6). SI activity was assayed by the method of Messer and Dahlquist (45), modified by using a glucose oxidase-peroxidase reagent that contains 4-aminoantipyrine instead of *o*-dianisidine as the chromogen (62). γ-Glutamyltranspeptidase (γ-GTP) activity was assayed by the method of Naftalin et al. (50). Alkaline phosphatase (AP) activity was assayed as described by Eichholz (19). Amino peptidase N (APN) and DPP IV were assayed as described by Maroux et al. (41) and Nagatsu et al. (51), respectively. Controls to exclude the possibility that an RRV protein could specifically inhibit the in vitro SI assay were performed. A lysate of noninfected cells was incubated with increased quantities of virus or with increased quantities of a lysate of infected cells. In either case, no decrease of SI activity of the control cell lysate was detected. Enzyme specific activities are expressed as milliunits/milligram of protein (mean ± standard deviation [SD]). One unit is defined as the activity that hydrolyzes 1 μmol of substrate/min at 37°C. Protein concentration was determined by the bicinchoninic acid assay.

Pulse-chase experiments. Filter-grown Caco-2 cells, mock infected or infected with RRV for 16 h, were incubated for two 30-min periods in DMEM without methionine-cysteine and then pulsed for 1 h with the same medium (150 μl/filter) containing 160 μCi of L-[^{35}S]methionine (via the basolateral side). After a wash with DMEM, the incorporated radioactivity was chased in DMEM containing 1 mM methionine and 2.5 mM cysteine for the indicated time.

Selective cell surface biotinylation. At the end of the chase period, cells were biotinylated at the apical or basolateral surface with NHS-LC-biotin (0.5 mg/ml diluted from a 200-mg/ml stock solution in dimethyl sulfoxide) as described previously (37). Biotinylation was performed twice on ice (20 min each time) and stopped by repeated washing with PBS and 50 mM NH_4Cl.

Immunoprecipitation, streptavidin precipitation, and SDS-PAGE. After biotinylation, filters were excised and cell homogenates were processed for immunoprecipitation using specific antibodies and protein A-Sepharose beads as previously described (3, 22). After immunoprecipitation, a 1/10 aliquot was directly analyzed to quantify the total amount of immunopurified antigens, and biotinylated proteins were recovered with streptavidin agarose beads from the remaining 9/10 of immunopurified antigens as described by LeBivic et al. (37). Immunopurified antigens and biotinylated proteins were analyzed by sodium dodecyl sulfate-polyacrylamide gel electrophoresis (SDS-PAGE) on a 7.5% or 6 to 15% polyacrylamide gel, and fluorography was performed as described by Sapin et al. (59). Fluorograms were quantified with a densitometric scanner (AGFA ARCUS II) and Image 1.57 software.

Viral protein detection. During RRV infection, viral proteins are oversynthesized and adhere nonspecifically to the protein A-Sepharose beads used to recover antibody-antigen complexes. Therefore, VP4 rotavirus proteins, in addition to hydrolases that are specifically immunoprecipitated, were always detected by SDS-PAGE. These background bands did not interfere with the detection of SI. However, there is an overlap between the molecular masses (each 100 kDa) of the high-mannose form (immature form) of DPP IV and of VP4. As high-mannose DPP IV is endo H sensitive whereas VP4 is endo H resistant, we performed endo H digestion (according to the manufacturer recommendations) to increase the mobility of digested high-mannose DPP IV. After endo H digestion, the high-mannose form of DPP IV became deglycosylated and its molecular mass decreased to 85 kDa, whereas the molecular mass of viral VP 4 did not change.

Antibodies and lectin. Rabbit polyclonal antirotavirus antibody 8148 was a gift from Jean Cohen. Rabbit polyclonal anti-human SI antibodies were a gift from Isabelle Chantret (Institut National de la Santé et de la Recherche Médicale [INSERM], Villejuif, France) (61). Rat anti-human DPP IV monoclonal antibody (MAb) 4H3 and rat anti-human SI MAb 8A9 were a gift from Suzanne Maroux (INSERM, Marseille, France) (25). Rabbit polyclonal anti-human villin antibody was a gift from Daniel Louvard (Institut Curie, Paris, France) (12). Fluorescein isothiocyanate (FITC)-conjugated rabbit anti-rat immunoglobulin G (IgG) was purchased from Sigma. Tetramethyl rhodamine (TRITC)-conjugated goat anti-rabbit IgG was from Biosys (Compiègne, France). FITC-conjugated goat anti-mouse IgG was purchased from Jackson ImmunoResearch Laboratories via Interchim. FITC-conjugated phalloidin was obtained from Molecular Probes via Interchim.

Immunofluorescence (IF) and CLSM. Caco-2 cells cultured on Transwell filters were fixed with 2% paraformaldehyde for 15 min at room temperature, washed three times with PBS, and then permeabilized with 0.2% Triton X-100 in H_2O. After three washes in PBS, cells were stained for SI, DPP IV, RRV, F-actin, or villin by incubation with the antibodies or lectin as described above for 60 min at room temperature. After three washes in PBS, cells were incubated with FITC- or TRITC-conjugated secondary antibody for 45 min. Following three washes in PBS, cells were incubated for 10 min with DABCO antifading reagent and mounted with Glycergel. Fluorescence was observed in a LEICA TCS equipped with a DMR inverted microscope and a 63/1.4 objective. A krypton-argon mixed-gas laser was used to generate two bands: 488 nm for FITC and 568 nm for TRITC. A band-pass filter was used to recover FITC fluorescence, and an LP 590 was used for TRITC. Both fluorochromes were excited and analyzed in one pass with no interference between the two channels. Image processing was performed with the on-line Scan Ware software. Numeric images were transferred to a Power Mac 8100 equipped with an image analysis station (Image 1.57 and Photoshop), and mounted images were printed on a Kodak XLS 8600 PS printer.

RESULTS

Selective decrease in SI activity and expression in RRV-infected Caco-2 cells. To characterize disaccharidase abnor-

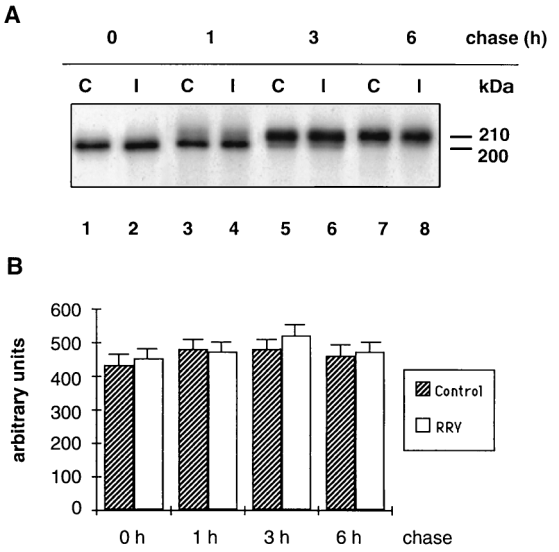

FIG. 3. SI biosynthesis, maturation, and stability in RRV-infected Caco-2 cells. At 16 h p.i., RRV-infected (I) and mock-infected (C) Caco-2 cells were pulse-labeled for 1 h with [^{35}S]methionine-cysteine and chased for 0, 1, 3, and 6 h. Cells were then extracted, and SI was detected by immunoprecipitation with an anti-SI MAb followed by SDS-PAGE (7.5% gel) and fluorography (A). (B) Densitometric quantification of the fluorogram shown in panel A. Values are means ± SD of three independent experiments.

malities induced by rotavirus infection of intestinal epithelial cells, we studied the activities of several brush border enzymes in RRV-infected Caco-2 cells. In these experiments, RRV-infected cells, detected by IF staining of viral antigens, represented 80% of the monolayer (Fig. 1B). In accordance with our previous work (34), no cell desquamation or destruction was observed at the level of phase-contrast microscopy (Fig. 1B). At 24 h p.i., RRV-infected Caco-2 cells were assayed for total membrane-associated SI, γ-GTP, AP, APN, and DPP IV activities. As seen in Fig. 1A, only SI activity was markedly affected by RRV infection. Its specific activity decreased by 66% of control values. No significant changes were observed in the activities of DPP IV, AP, APN, and γ-GTP.

Indirect IF staining and CLSM experiments were conducted to investigate whether alterations in SI distribution were associated with its decreased activity. At 24 h p.i., RRV-infected Caco-2 cells were fixed with paraformaldehyde, permeabilized with Triton X-100, and labeled with anti-SI or anti-DPP IV antibodies. In Caco-2 control cells, horizontal sections (XY) of the apical region (Fig. 2A) showed normal SI staining (30, 55). Vertical sections perpendicular to the plane of the monolayer (XZ) showed, as expected, that SI staining was exclusively localized at the apical domain of Caco-2 cells. In RRV-infected cells, SI staining was strikingly decreased at the apical surface of the cells (Fig. 2A). This observation was confirmed on XZ sections of the same monolayer. In contrast, the apical expression of DPP IV, which does not exhibit decreased activity upon RRV infection, was the same as for control cells (Fig. 2B). However, the basolateral expression of DPP IV was greater in infected cells than in control cells.

Altogether, these results demonstrate that the selective low level of SI activity induced by RRV infection is associated with a specific reduction of SI expression at the apical domain of Caco-2 cells and does not result from enterocytic destruction.

Effect of RRV infection on biosynthesis, maturation, and stability of SI. To define which step(s) of SI processing is altered by RRV infection, we used ^{35}[S]methionine pulse-chase experiments to study the biosynthesis, maturation, and stability of SI and of DPP IV. Infected and mock-infected Caco-2 cells were pulse-labeled for 1 h and then chased for various time periods. SI and DPP IV were quantitatively immunoprecipitated and analyzed by SDS-PAGE.

In Caco-2 control cells, biosynthesis and processing of SI followed the same kinetics as previously described (30, 43). After 30 min of chase, SI was present in the 200-kDa band representing the high-mannose form. After 1 h of chase, a small fraction was processed to the 210-kDa complex form. This fraction increased after 3 h of chase and was the only SI form after a 6-h chase period (Fig. 3A, lanes C). RRV-infected Caco-2 cells exhibited an identical pattern of SI synthesis. Furthermore, densitometric scanning of the fluorogram indicates that RRV-infected cells synthesized the same amount of SI as did control Caco-2 cells (Fig. 3B). SI processing in RRV-infected cells also followed the same patterns and kinetics as in control cells (Fig. 3A). These findings indicate that SI biosynthesis, maturation, and stability are not impaired in RRV-infected cells.

DPP IV biosynthesis, maturation, and stability were examined by comparison. In control Caco-2 cells receiving a 1-h pulse, newly synthesized DPP IV was expressed as the immature 100-kDa high-mannose form, which was processed to the 110-kDa complex glycosylated form following a chase for 1 to 6 h (Fig. 4A, lanes C). For RRV-infected cells, as mentioned in Materials and Methods, interpretation of the gel was complicated by viral VP4 protein migrating at the same position as

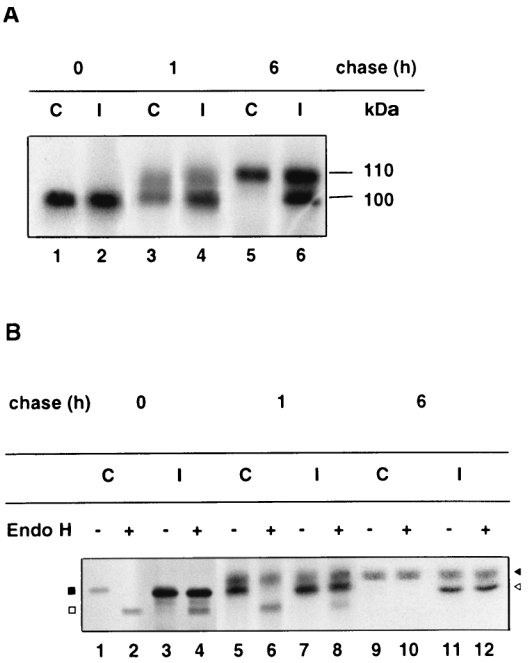

FIG. 4. DPP IV biosynthesis, maturation, and stability in RRV-infected cells. After the immunoprecipitation with an anti-SI MAb (Fig. 3), the supernatants depleted of SI were immunoprecipitated with an anti-DPP IV MAb. The immunoprecipitates were then analyzed by SDS-PAGE on a 6 to 15% (A) or 7.5% (B) polyacrylamide gel without endo H treatment (panel B, lanes 1, 3, 5, 7, 9, and 11) or after endo H treatment (panel B, lanes 2, 4, 6, 8, 10, and 12) in order to differentiate the high-mannose DPP IV form from viral protein VP4 as described in Materials and Methods. After endo H treatment, the immature form of DPP IV became deglycosylated and its molecular mass decreased to 85 kDa, whereas the molecular mass of VP4 did not change. Labeled proteins were visualized by fluorography (black square, immature 100-kDa DPP IV; white square, deglycosylated 85-kDa DPP IV; black arrowhead, mature 110-kDa DPP IV; white arrowhead, viral protein VP4). I, RRV-infected Caco-2 cells; C, mock-infected Caco-2 cells.

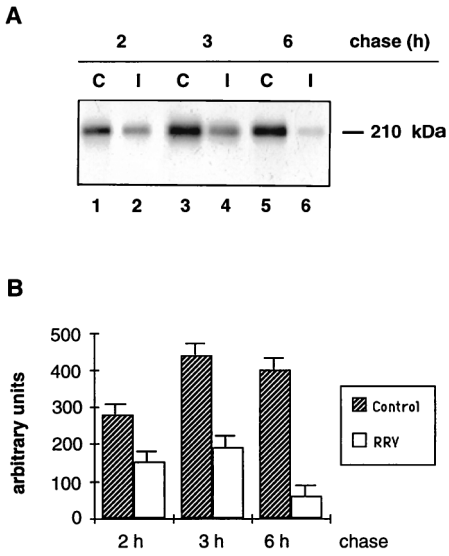

FIG. 5. Delivery of SI to the apical surface is blocked by RRV infection. At 16 h p.i., RRV-infected (I) and mock-infected (C [control]) Caco-2 cells were pulse-labeled for 1 h with [^{35}S]methionine-cysteine and chased for 2, 3, or 6 h. The monolayers were then biotinylated on the apical surfaces and extracted, and SI reaching the apical surface was determined by immunoprecipitation, streptavidin precipitation, SDS-PAGE (7.5% gel), and fluorography. (A) SI apical arrival; (B) densitometric quantification of the fluorogram in panel A. Values are means ± SD of three independent experiments.

the immature 100-kDa high-mannose DPP IV form (Fig. 4A, lanes I). Therefore, to differentiate between these two proteins, we performed endo H experiments. As shown in Fig. 4B, the amount of DPP IV as well as the maturation patterns and kinetics of the enzyme were the same in RRV-infected cells as in control cells (Fig. 4B; compare lanes 2, 6, and 10 [control] with lane 4, 8, and 12 [infected cells]).

These results show that RRV infection does not perturb SI or DPP IV biosynthesis, stability, and maturation rates.

Effect of RRV infection on delivery of SI to the cell surface. We next studied cell surface delivery of SI and DPP IV in RRV-infected Caco-2 cells by radioactive pulse-chase and selective surface domain biotinylation.

In agreement with previous studies (36, 42), SI accumulation at the apical domain of control cells increased progressively during a 2- to 6-h chase (Fig. 5A). SI was barely detectable at the basolateral side of Caco-2 cells (not shown). In RRV-infected cells, while SI was still undetectable at the basolateral surface (not shown), the amount present at the apical surface was much less than in control cells (Fig. 5A). Scanning of the fluorograms (Fig. 5B) confirmed that apical expression of SI was greatly reduced following a 6-h chase.

DPP IV membrane delivery was also examined. In control cells, its polarized cell surface delivery followed essentially the same pattern and kinetics as previously reported (42). The enzyme was first inserted into both apical and basolateral cell surface domains. During 3 to 6 h of chase, DPP IV decreased at the basolateral surface but increased in the apical membrane, compatible with its rapid transcytosis to the apical surface (42) (Fig. 6A). In RRV-infected cells, while the total amount of membrane DPP IV was the same as in control cells, its pattern and kinetics of domain-specific expression were different (Fig. 6A). After a 3-h chase (by which time DPP IV was entirely processed and migrated as the upper 110-kDa band), the amount of newly synthesized DPP IV in the apical membrane of RRV-infected cells was slightly lower than in control cells (30% of the total membrane DPP IV, versus 40% in control cells). Moreover, between 3 and 6 h of chase, the amount of DPP IV delivered to the apical surface via transcytosis from the basolateral pole increased by 7% in RRV-infected cells, compared to 24% in control cells (Fig. 6B). However, after an overnight chase, the level of apical DPP IV reached control values in infected cells (Fig. 6). These results show that RRV infection induced an almost complete blockade of SI targeting to the apical surface, while apical DPP IV targeting was only delayed.

RRV infection perturbs the organization of microvillar cytoskeleton in Caco-2 cells. Alteration of brush border-associated cytoskeleton has been shown to impair apical SI expression (12, 58). For this reason, we used CLSM to study the spatial distribution of two major brush border-associated cytoskeleton components, actin microfilaments and villin, an actin-associated protein, in RRV-infected Caco-2 cells. At 24 h p.i., RRV-infected and mock-infected Caco-2 cells were fixed, permeabilized, and stained with phalloidin-fluorescein, which specifically binds to F-actin, or stained with a monoclonal antivillin antibody. Selected horizontal sections from the apex to the base of the cells are shown in Fig. 7 and 8.

In control cells, most F-actin was localized within the apical

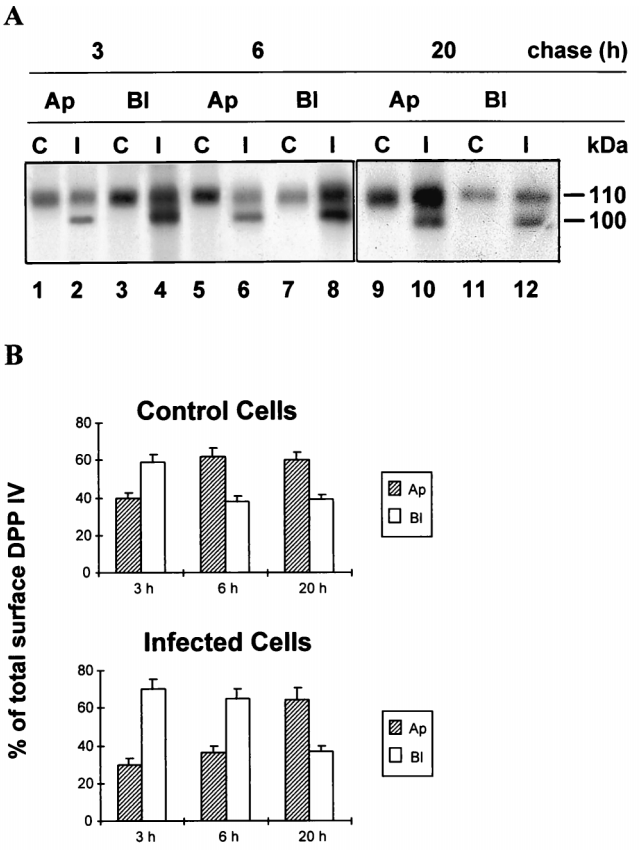

FIG. 6. Apical and basolateral delivery of DPP IV is delayed by RRV infection. After immunoprecipitation with an anti-SI MAb (Fig. 5), the supernatants depleted of SI were immunoprecipitated with an anti-DPP IV MAb. Apical (Ap) and basolateral (Bl) biotinylated DPP IV were subjected to streptavidin precipitation, SDS-PAGE (15% gel), and fluorography. After a 3-h chase, DPP IV was entirely processed to the 110-kDa complex glycosylated form and represented only by the upper 110-kDa band. The 100-kDa band represents the viral protein VP 4 (A). (B) Densitometric quantification of the DPP IV bands shown in panel A. Values are means ± SD of three independent experiments. C, control; I, infected.

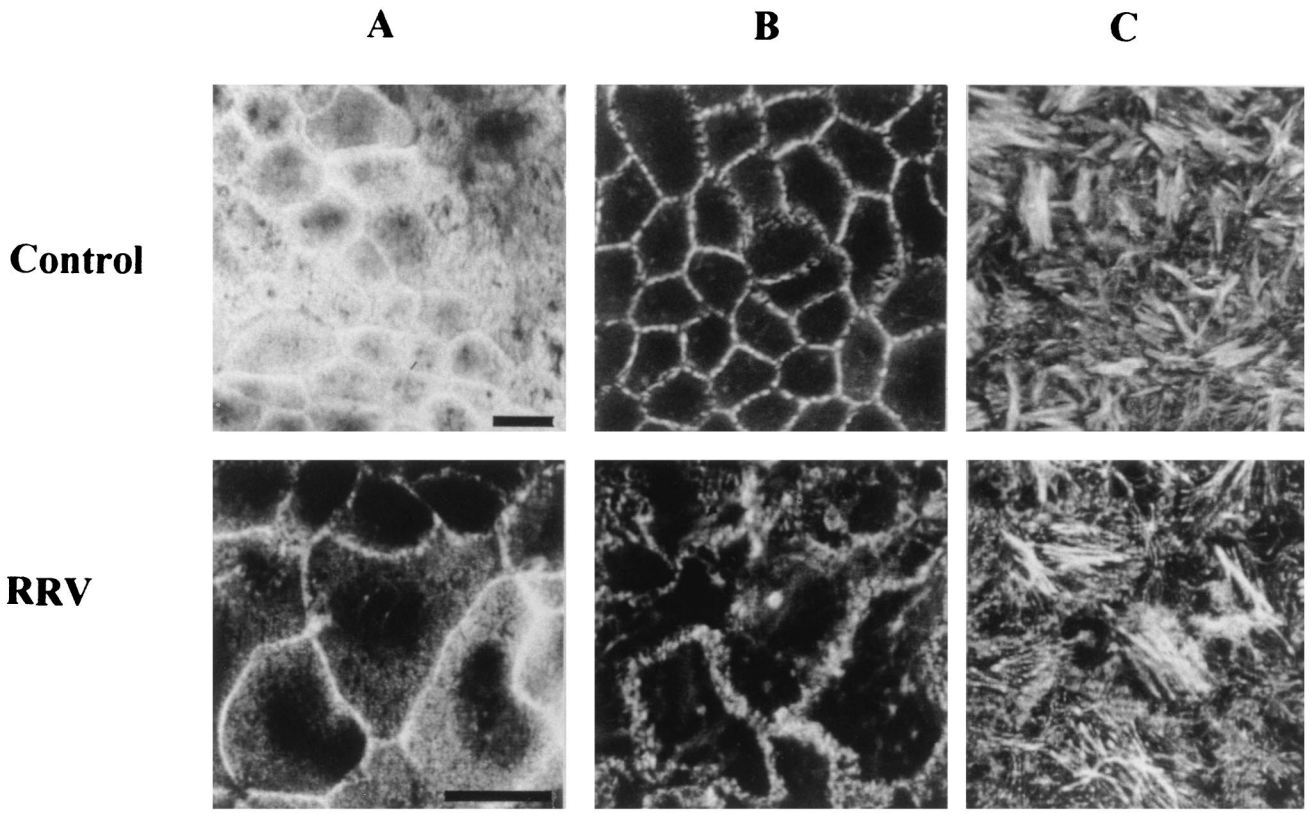

FIG. 7. Three-dimensional F-actin alteration induced by RRV infection. At 24 h p.i., RRV-infected and mock-infected Caco-2 cells were fixed, permeabilized, and stained with fluorescein-phalloidin, which binds to F-actin. Horizontal sections were generated by CLSM along an axis perpendicular to the monolayer, at the apex (A), the middle (B), and the base (C) of the cell. Bars, 10 μm.

domain (Fig. 7A). Only weak staining of microfilaments was observed along the lateral membrane (Fig. 7B), and stress fibers were poorly represented in the basal region, as is usual for confluent Caco-2 cells (Fig. 7C). In RRV-infected cells, the F-actin staining completely disappeared from the apex of the cells (Fig. 7A). Lateral F-actin and basal stress fibers were only slightly affected (Fig. 7B and C) compared to control cells. Villin expression was also strongly altered by infection (Fig. 8). Apical staining had, to a great extent, disappeared (Fig. 8A), and subcortical staining appeared irregular and organized into patches (Fig. 8B) compared to control cells. Altogether, these results show that RRV infection induces significant changes in the distribution of brush border-associated cytoskeletal proteins in polarized intestinal Caco-2 cells.

DISCUSSION

Rotavirus infection is known to reduce the level of disaccharidase activity in intestinal epithelial cells in vivo. In this study, we used the human intestinal epithelial cell line Caco-2 to demonstrate that RRV infection specifically and selectively decreased the activity and apical expression of SI without altering activity and apical expression of other brush border hydrolases. This alteration occurs without apparent cell destruction, a result that confirms our previous finding that RRV can replicate and be released from intestinal epithelial cells without cell lysis (34). We also demonstrate that the reduction of SI apical expression was due to a block in its transport from the TGN to the brush border membrane. Finally, we show that RRV infection perturbs the brush border-associated cytoskeleton, which may explain the block in SI transport to the apical surface.

In 1977, Davidson and collaborators proposed a mechanism to explain the low level of disaccharidase activity induced by rotavirus infection; they hypothesized that the enterocytes that repopulate the villi after virus-induced tip cell destruction could be crypt-like, with a reduced digestive capacity (18). However, this mechanism cannot account for the low disaccharidase activities that are still observed in rotavirus-infected enterocytes exhibiting little, if any, cytopathological abnormalities (4, 17). Interestingly, recent in vivo results have led to the conclusion that disaccharidase deficiency could not result from repopulation of villi with immature enterocytes but more likely reflected a specific functional alteration of infected enterocytes (10). Using the intestinal epithelial cell line Caco-2, we clearly show that decrease of SI activity did not result from enterocyte or brush border destruction. Furthermore, DPP IV shows a normal enzymatic activity and is correctly expressed at the apical surface of RRV-infected cells. These results are consistent with decrease of disaccharidase activity observed in vivo in the absence of enterocyte destruction and any physiopathologic changes (4, 10, 17).

Our results show that rotavirus infection perturbs the last step of SI processing, transport from the TGN to the brush border. Polarized transport of membrane proteins in epithelial cells involves carrier vesicles, the specific fusion of these vesicles with the appropriate membrane domain, and protein retention across the membrane. RRV infection may interfere with such mechanisms. However, while intracellular transport of SI to the brush border was dramatically impaired upon RRV

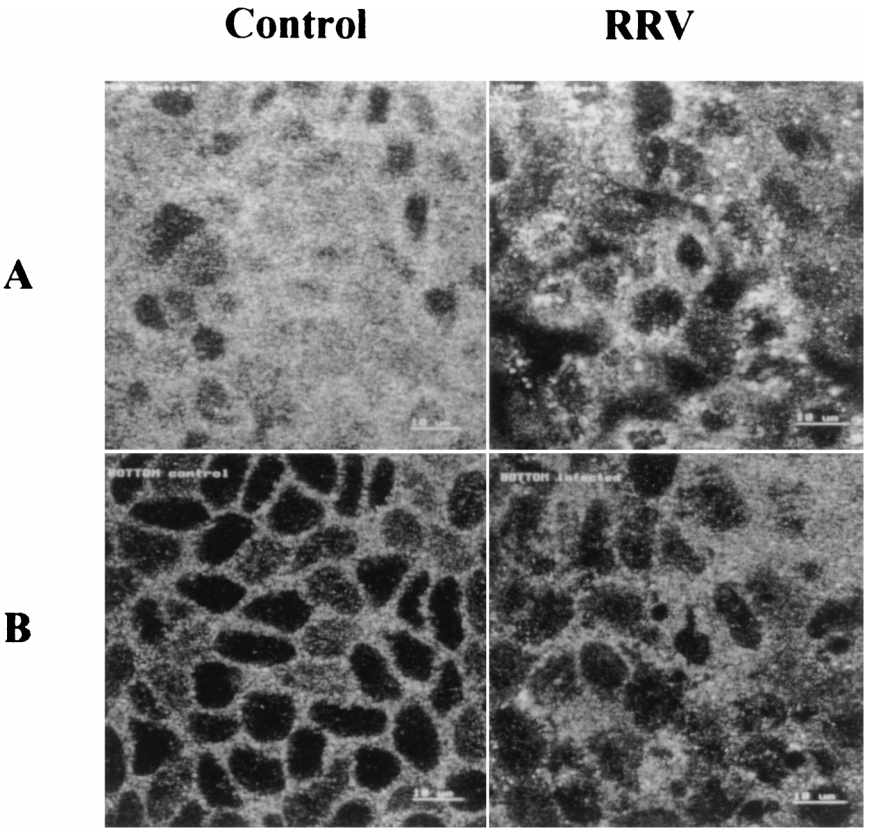

FIG. 8. Alteration of villin organization induced by RRV infection. At 24 h p.i., RRV-infected and mock-infected Caco-2 cells were fixed, permeabilized, and immunostained with polyclonal antivillin antibodies and fluorescein-labeled anti-rabbit IgG antibodies. Apical (A) and subcortical (B) horizontal sections were generated by CLSM. Bars, 10 μm.

infection, DPP IV arrival to the brush border was merely delayed. This difference in effect may account for the different apical transport pathways followed by the two enzymes. Indeed, SI is targeted directly to the apical membrane (36, 42), whereas DPP IV is first inserted into the basolateral membrane and subsequently retrieved by transcytosis to the apical surface (42). Moreover, SI but not DPP IV has been detected in Triton X-100-resistant microdomains of glycosphingolipids (GSL) (22) in charge of the direct transport of glycosylphosphatidylinositol-anchored proteins from the TGN to the apical membrane (22, 39). Interestingly, we previously observed that RRV was transported and released at the apical membrane of Caco-2 cells by vesicular transport (34). Furthermore, preliminary studies from our laboratory have shown that in infected Caco-2 cells, RRV proteins are detected in the Triton X-100-insoluble fraction (unpublished data), suggesting that rotavirus-containing vesicles interact with GSL microdomains. Further studies will determine if rotavirus interferes with the apical transport of SI by perturbing these GSL microdomains.

Another hypothesis to explain the specific reduction in SI expression at the apical surface involves reorganization of the microvillar cytoskeleton. Costa de Beauregard and collaborators (12) used an antisense RNA strategy to inhibit synthesis of villin. The results of these experiments showed that the brush border microvilli were disassembled. Furthermore, concomitantly apical localization of SI, but not other brush border enzymes, was specifically impaired. Salas and collaborators have also disorganized the microvillar cytoskeleton by reducing expression of cytokeratin 19; this also perturbed apical targeting for SI as well as AP (58). In MDCK cells, the protein gp135 is maintained on the apical cell surface through interaction with actin microfilaments of the apical cytoskeleton (53). In the same cellular model, preferential basolateral retention of Na^+,K^+-ATPase is due to ankyrin and fodrin, two actin-binding proteins of the basolateral membrane cytoskeleton (27, 52). The apical actin and villin disassembly induced by RRV infection is in accordance with the aberrantly shaped microvilli observed in RRV-infected Caco-2 cells by electron microscopy (34) and could also explain the block in apical SI transport.

In many viral infections, alterations of the cytoskeleton are caused by a direct interaction between virus or viral proteins and components of the cytoskeleton, thus contributing to replication, assembly, transport, and/or release of virions (1, 14, 49, 63). Two RNA-binding nonstructural proteins of rotavirus, NSP1 and NSP2, associate with the cytoskeleton (32, 44), suggesting that replication and/or capsid assembly may require a cytoskeleton framework. In our study, microvillus cytoskeleton changes were observed at a late stage of infection (from 16 [not shown] to 24 h p.i.), corresponding to the release of virions. Therefore, interaction between rotavirus and components of microvillus cytoskeleton during virion release is possible. Another possibility is that rotavirus infection indirectly changes the organization of the cytoskeleton through biochemical events. For example, increase of intracytoplasmic calcium is caused by rotavirus infection (46, 60) and is known to induce disassembly and alterations in microvilli (31, 47, 48). It is thus conceivable that rotavirus infection can trigger cytoskeleton alteration by a Ca^{2+}-dependent mechanism. Such a mecha-

nism would be in accordance with the new concept of viral enterotoxin proposed by Ball and collaborators (2) for the rotavirus nonstructural glycoprotein NSP4. Indeed, NSP4 is capable of inducing dose-related diarrhea in young CD1 mice by stimulating a Ca^{2+}-dependent pathway that would alter intestinal epithelial transport (2).

In conclusion, Caco-2 cells have proved to be a powerful enterocyte-like model with which to study mechanisms by which rotavirus infection induces alterations in disaccharidase activities. In the absence of enterocyte destruction, rotavirus infection induces a specific alteration of SI arrival to the apical surface that may involve interaction with GSL transport or/and the microvillus cytoskeleton. Our results provide an alternate model of rotavirus pathophysiology.

ACKNOWLEDGMENTS

We thank J. Cohen (INRA, Jouy en Josas, France) for kindly providing antirotavirus serum and the RRV strain. We thank I. Chantret (INSERM, Villejuif, France) for generously providing anti-SI serum and S. Maroux (INSERM, Marseille, France) for the gift of anti-SI MAb and anti-DPP IV MAb. We thank M. Vasseur for helpful advice concerning enzyme activities. We also thank M. Maurice, B. Wice, and T. Karjalainen for helpful discussions during preparation of the manuscript. Most of the confocal experiments were performed with the kind cooperation of the Institut Fédératif de Recherche INSERM "Cellules Epithéliales" (CHU Xavier Bichat, Paris, France).

REFERENCES

1. **Alves de Matos, A. P., and Z. G. Carvalho.** 1993. African swine fever virus interaction with microtubules. Biol. Cell **78:**229–234.
2. **Ball, J. M., P. Tian, C. Q.-Y. Zeng, A. P. Morris, and M. K. Estes.** 1996. Age-dependent diarrhea induced by a rotaviral nonstructural glycoprotein. Science **272:**101–104.
3. **Baricault, L., M. Garcia, C. Cibert, C. Sapin, G. Geraud, P. Codogno, and G. Trugnan.** 1993. Forskolin blocks the apical expression of dipeptidyl peptidase IV in Caco-2 cells and induces its retention in lamp-1-containing vesicles. Exp. Cell Res. **209:**277–287.
4. **Barnes, G. L., and R. R. W. Townley.** 1973. Duodenal mucosal damage in 31 infants with gastroenteritis. Arch. Dis. Child. **48:**343–349.
5. **Bishop, R. F., G. P. Davidson, I. H. Holmes, and B. J. Ruck.** 1973. Virus particles in epithelial cells of duodenal mucosa from children with acute non-bacterial gastroenteritis. Lancet **2:**1281–1283.
6. **Blais, A., P. Bissonnette, and A. Berteloot.** 1987. Common characteristics for Na-dependent sugar transport in Caco-2 cells and human fetal colon. J. Membr. Biol. **99:**113–125.
7. **Broyart, J. P., J. P. Hugot, C. Perret, and A. Porteu.** 1990. Molecular cloning and characterization of rat intestinal sucrase-isomaltase cDNA. Regulation of sucrase-isomaltase gene expression by sucrose feeding. Biochim. Biophys. Acta **1087:**61–67.
8. **Chantret, I., G. Trugnan, E. Dussaulx, A. Zweibaum, and M. Rousset.** 1988. Monensin inhibits the expression of sucrase-isomaltase in Caco-2 cells at the mRNA level. FEBS Lett. **235:**125–128.
9. **Clark, S. M., J. R. Roth, M. L. Clark, B. B. Barnett, and R. S. Spendlove.** 1981. Trypsin enhancement of rotavirus infectivity: mechanism of enhancement. J. Virol. **39:**816–822.
10. **Collins, J., D. C. A. Candy, W. G. Starkey, A. J. Spencer, M. P. Osborne, and J. Stephen.** 1990. Disaccharidase activities in small intestine of rotavirus-infected suckling mice: a histochemical study. J. Pediatr. Gastroenterol. Nutr. **11:**395–403.
11. **Collins, J., W. G. Starkey, T. S. Wallis, G. J. Clarke, K. J. Worton, A. J. Spencer, S. J. Haddon, M. P. Osborne, D. C. A. Candy, and J. Stephen.** 1988. Intestinal enzyme profiles in normal and rotavirus-infected mice. J. Pediatr. Gastroenterol. Nutr. **7:**264–272.
12. **Costa de Beauregard, M.-A., E. Pringault, S. Robine, and D. Louvard.** 1995. Suppression of villin expression by antisense RNA impairs brush border assembly in polarized epithelial intestinal cells. EMBO J. **14:**409–421.
13. **Cross, H. S., and A. Quaroni.** 1991. Inhibition of sucrase-isomaltase expression by EGF in the human colon adenocarcinoma cells Caco-2. Am. J. Physiol. **261:**C1173–1183.
14. **Cudmore, S., P. Cossart, G. Griffiths, and M. Way.** 1995. Actin-based motility of vaccinia virus. Nature **378:**636–638.
15. **Danielsen, E. M.** 1992. Folding of intestinal brush border enzymes. Evidence that high-mannose glycosylation is an essential early event. Biochemistry **31:**2266–2272.
16. **Danielsen, E. M.** 1989. Post-translational suppression of expression of intestinal brush border enzymes by fructose. J. Biol. Chem. **264:**13726–13729.
17. **Davidson, G. P., and G. L. Barnes.** 1979. Structural and functional abnormalities of the small intestine in infants and young children with rotavirus enteritis. Acta Paediatr. Scand. **68:**181–186.
18. **Davidson, G. P., G. Gall, M. Petric, D. Butler, and J. R. Hamilton.** 1977. Human rotavirus enteritis induced in conventional piglets. J. Clin. Invest. **60:**1402–1409.
19. **Eichholz, A.** 1967. Structural and functional organization of the brush border of intestinal epithelial cells. III. Enzymic activities and chemical composition of various fractions of tris-disrupted brush borders. Biochim. Biophys. Acta **135:**475–482.
20. **Fogh, J., J. M. Fogh, and T. Orfeo.** 1977. One hundred and twenty seven cultured human tumor cell lines producing tumor in nude mice. J. Natl. Cancer Inst. **59:**221–226.
21. **Fransen, J. A. M., H. P. Hauri, L. A. Ginsel, and H. Y. Naim.** 1991. Naturally occurring mutations in intestinal sucrase-isomaltase provide evidence for existence of an intracellular sorting signal in the isomaltase subunit. J. Cell Biol. **115:**45–57.
22. **Garcia, M., C. Mirre, A. Quaroni, H. Reggio, and A. LeBivic.** 1993. GPI-anchored proteins associate to form microdomains during their intracellular transport in Caco-2 cells. J. Cell Sci. **104:**1281–1290.
23. **Goda, T., and O. Koldovsky.** 1988. Dietary regulation of small intestinal disaccharidases. World Rev. Nutr. Diet **57:**275–329.
24. **Goda, T., F. Raul, F. Gosse, and O. Koldovsky.** 1988. Effects of a high protein, low carbohydrate diet on degradation of sucrase-isomaltase in rat jejunoileum. Am. J. Physiol. **254:**907–912.
25. **Gorvel, J. P., A. Ferrero, L. Chanbraud, A. Rigal, J. Bonicel, and S. Maroux.** 1991. Expression of sucrase-isomaltase and dipeptidylpeptidase IV in human small intestine and colon. Gastroenterology **101:**618–625.
26. **Greenberg, H. B., H. F. Clark, and P. A. Offit.** 1994. Rotavirus pathology and pathophysiology. Curr. Top. Microbiol. Immunol. **185:**256–283.
27. **Hammerton, R. W., K. A. Krzeminski, R. W. Mays, T. A. Ryan, D. A. Wollner, and W. J. Nelson.** 1991. Mechanism for regulating cell surface distribution of Na+, K+-ATPase in polarized epithelial cells. Science **254:**847–850.
28. **Hauri, H. P.** 1988. Biogenesis and intracellular transport of intestinal brush border membrane hydrolase. Use antibody probes and tissue culture, p. 155–219. *In* J. R. Harris (ed.), Subcellular biochemistry and immunological aspects, vol. 12. Plenum, New York, N.Y.
29. **Hauri, H. P., J. Roth, E. E. Sterchi, and M. J. Lentze.** 1985. Transport to cell surface of intestinal sucrase-isomaltase is blocked in the Golgi apparatus in a patient with congenital sucrase-isomaltase deficiency. Proc. Natl. Acad. Sci. USA **82:**4423–4427.
30. **Hauri, H. P., E. E. Sterchi, D. Bienz, J. A. M. Fransen, and A. Marxer.** 1985. Expression and intracellular transport of microvillus membrane hydrolases in human intestinal epithelial cells. J. Cell Biol. **101:**838–851.
31. **Howe, C. L., M. S. Mooseker, and T. A. Graves.** 1980. Brush-border calmodulin: a major component of the isolated microvillus core. J. Cell Biol. **85:**916–923.
32. **Hua, J., and J. Patton.** 1994. The carboxyl-half of the rotavirus nonstructural protein NS53 (NSP1) is not required for virus replication. Virology **198:**567–576.
33. **Hunziker, W., M. Spiess, G. Semenza, and H. F. Lodish.** 1986. The sucrase-isomaltase complex: primary structure, membrane orientation, and evolution of a stalked, intrinsic brush-border protein. Cell **46:**227–234.
34. **Jourdan, N., M. Maurice, D. Delautier, A. M. Quero, A. L. Servin, and G. Trugnan.** 1997. Rotavirus is released from the apical surface of cultured human intestinal cells through nonconventional vesicular transport that bypasses the Golgi apparatus. J. Virol. **71:**8268–8278.
35. **Kapikian, A. Z., and R. M. Chanock.** 1996. Rotaviruses, p. 1657–1708. *In* B. N. Fields and D. M. Knipe (ed.), Fields' virology. Raven Press, New York, N.Y.
36. **LeBivic, A., A. Quaroni, B. Nichols, and E. Rodriguez-Boulan.** 1990. Biogenetic pathways of plasma membrane proteins in Caco-2, a human intestinal epithelial cell line. J. Cell Biol. **111:**1351–1361.
37. **LeBivic, A., F. X. Real, and E. Rodriguez-Boulan.** 1989. Vectorial targeting of apical and basolateral plasma membrane proteins in a human adenocarcinoma epithelial cell line. Proc. Natl. Acad. Sci. USA **86:**9313–9317.
38. **Leeper, L. L., and S. J. Henning.** 1990. Development and tissue distribution of sucrase-isomaltase mRNA in rats. Am. J. Physiol. **258:**52–58.
39. **Lisanti, M. P., and E. Rodriguez-Boulan.** 1990. Glycolipids membrane anchoring provides clues to mechanism of protein sorting in polarized epithelial cells. Trends Biochem. Sci. **15:**113–118.
40. **Lloyd, M. L., and W. A. Olsen.** 1987. A study of the molecular pathology of sucrase-isomaltase deficiency. N. Engl. J. Med. **316:**438–442.
41. **Maroux, S. D., D. Louvard, and J. Battari.** 1973. The aminopeptidase from hog intestinal brush border. Biochim. Biophys. Acta **321:**282–295.
42. **Matter, K., M. Brauchbar, K. Bucher, and H. P. Hauri.** 1990. Sorting of endogenous plasma membrane proteins occurs from two sites in cultured human intestinal epithelial cells (Caco-2). Cell **60:**429–437.
43. **Matter, K., and H. P. Hauri.** 1991. Intracellular transport and conformational maturation of intestinal brush border hydrolases. Biochemistry **30:**1916–1923.

44. **Mattion, N. M., J. Cohen, C. Aponte, and M. K. Estes.** 1992. Characterization of an oligomerization domain and RNA-binding properties on rotavirus nonstructural protein NS34. Virology **190:**68–83.
45. **Messer, M., and A. Dahlquist.** 1966. A one step ultramicromethod for the assay of disaccharidases. Anal. Biochem. **14:**372–392.
46. **Michelangeli, F., M.-C. Ruiz, J. R. Del Castillo, J. E. Ludert, and F. Liprandi.** 1991. Effect of rotavirus infection on intracellular calcium homeostasis in cultured cells. Virology **181:**520–527.
47. **Mooseker, M. S.** 1985. Organization, chemistry, and assembly of the cytoskeletal apparatus of the intestinal brush border. Annu. Rev. Cell Biol. **1:**209–241.
48. **Mooseker, M. S., T. A. Graves, K. A. Wharton, N. Falco, and C. L. Howe.** 1980. Regulation of microvillus structure: calcium-dependent solation and cross-linking of actin filaments in the microvilli of intestinal epithelial cells. J. Cell Biol. **87:**809–822.
49. **Murti, K. G., and R. Goorha.** 1983. Interaction of Frog virus-3 with the cytoskeleton. I. Altered organisation of microtubules, intermediate filaments, and microfilaments. J. Cell Biol. **96:**1248–1257.
50. **Naftalin, L., M. Sexton, J. F. Whitaker, and R. J. Randall.** 1969. A routine procedure for estimating serum γ-glutamyltranspeptidase activity. Clin. Chim. Acta **26:**293–296.
51. **Nagatsu, T., M. Hino, H. Fuyamada, T. Hayakawa, S. Sakakibara, Y. Nakagawa, and T. Takemoto.** 1976. New chromogenic substrates for x-prolyl dipeptidyl aminopeptidase. Anal. Biochem. **74:**466–476.
52. **Nelson, W. J., and R. W. Hammerton.** 1989. A membrane-cytoskeletal complex containing Na+, K+-ATPase, ankirine and fodrin in Madin-Darby canine kidney (MDCK) cells: implications for the biogenesis of epithelial cell polarity. J. Cell Biol. **108:**893–902.
53. **Ojakian, G. K., and R. Schwimmer.** 1988. The polarized distribution of an apical cell surface glycoprotein is maintained by interactions with the cytoskeleton of Madin-Darby canine kidney cells. J. Cell Biol. **107:**2377–2387.
54. **Ouwendijk, J., C. E. C. Moolenaar, W. J. Peters, C. P. Hollenberg, L. A. Ginsel, J. A. M. Fransen, and H. Y. Naim.** 1996. Congenital sucrase-isomaltase deficiency. Identification of a glutamine to proline substitution that leads to transport block of sucrase-isomaltase in a pre-Golgi compartment. J. Clin. Invest. **97:**633–641.
55. **Pinto, M., S. Robine-Leon, M. D. Appay, M. Kedinger, N. Triadou, E. Dussaulx, B. Lacroix, P. Simon-Assman, K. Haffen, J. Fogh, and A. Zweibaum.** 1983. Enterocyte-like differentiation and polarization of the human colon carcinoma cell line Caco-2 in culture. Biol. Cell **47:**323–330.
56. **Quaroni, A., E. C. A. Paul, and B. L. Nichols.** 1993. Intracellular degradation and reduced cell-surface expression of sucrase-isomaltase in heat-shocked Caco-2 cells. Biochem. J. **292:**725–734.
57. **Rousset, M., I. Chantret, D. Darmoul, G. Trugnan, C. Sapin, F. Green, D. Swallow, and A. Zweibaum.** 1989. Reversible forskolin-induced impairment of sucrase-isomaltase mRNA levels, biosynthesis, and transport to the brush border membrane in Caco-2 cells. J. Cell. Physiol. **141:**627–635.
58. **Salas, P. J. I., M. L. Rodriguez, A. L. Viciana, D. E. Vegas-Salas, and H. P. Hauri.** 1997. The apical submembrane cytoskeleton participate in the organization of the apical pole in epithelial cells. J. Cell Biol. **137:**359–375.
59. **Sapin, C., L. Baricault, and G. Trugnan.** 1997. PKC-dependent long-term effect of PMA on protein cell surface expression in Caco-2 cells. Exp. Cell Res. **231:**308–318.
60. **Tian, P., Y. Hu, W. P. Shilling, D. A. Lindsay, J. Eiden, and M. K. Estes.** 1994. The nonstructural glycoprotein of rotavirus affects intracellular calcium levels. J. Virol. **68:**251–257.
61. **Trugnan, G., M. Rousset, I. Chantret, A. Barbat, and A. Zweibaum.** 1987. The posttranslational processing of sucrase-isomaltase in HT-29 cells is a function of their state of enterocyte differentiation. J. Cell Biol. **104:**1199–1205.
62. **Vasseur, M.** 1989. Purification of the rabbit small intestinal sucrase-isomaltase complex: separation from other maltases. Biosci. Rep. **9:**341–346.
63. **Volkman, L. E., and K. J. M. Zaal.** 1990. Autographica californica M nuclear polyhedrosis virus: microtubule and replication. Virology **175:**292–302.
64. **Yeh, K. Y., M. Yeh, and P. R. Holt.** 1989. Differential effects of thyroxine and cortisone on jejunal sucrase expression in suckling rats. Am. J. Physiol. **256:**604–612.